First-principles prediction of zone-center optical phonon linewidths and IR spectra of hexagonal boron nitride

Ziqi Guo,[1] Peter Sokalski,[2] Zherui Han,[1] Yanhua Cheng,[1] Li Shi,[2] Takashi Taniguchi,[3] Kenji Watanabe,[4] and Xiulin Ruan[1, a)]

[1)] *School of Mechanical Engineering and the Birck Nanotechnology Center, Purdue University, West Lafayette, 47907, IN, USA*

[2)] *Department of Mechanical Engineering, The University of Texas at Austin, Austin, 78712, TX, USA*

[3)] *Research Center for Materials Nanoarchitectonics, National Institute for Materials Science, 1-1 Namiki, Tsukuba 305-0044, Japan*

[4)] *Research Center for Electronic and Optical Materials, National Institute for Materials Science, 1-1 Namiki, Tsukuba 305-0044, Japan*

(Dated: 12 November 2024)

Raman and infrared (IR) spectra provide rich information about materials. In this study, we employ first-principles calculations to predict the temperature-dependent linewidths of zone-center phonon modes, along with the IR dielectric function in bulk hexagonal boron nitride. We include the contributions of three-phonon, four-phonon scattering, and phonon renormalization, and our predictions show good agreement with our own experimental results as well as those in the literature. Our findings show that the temperature dependency of phonon linewidth would be strengthened by considering four-phonon scattering while weakened by further including phonon renormalization. After considering all these effects, four-phonon scattering shows a significant or even leading contribution to the linewidth over three-phonon scattering, especially at elevated temperatures.

[a)] Electronic mail: ruan@purdue.edu

As a van der Waals crystal, hexagonal boron nitride (h-BN) has a layered structure similar to graphite and features a strong crystalline anisotropy. Consequently, the dielectric permittivity of h-BN shows opposite signs along orthogonal axes, making it a low-loss natural hyperbolic material[1–3]. This feature is key to optoelectronic, nanophotonic and phonon-polariton applications[2,4–7], including quantum emitter[6,8], single-photon sources[9], super-resolution imaging[10], nanolithography[11], and radiative cooling[12].

Several experimental measurements have been conducted to characterize the dielectric function, Raman spectra, and infrared (IR) spectra of h-BN at room temperature[1,13–16]. However, the measurement of optical linewidth and dielectric function at high temperatures is hindered by issues such as thermal oxidation and self-radiation[17], and few measurements have been reported. A comprehensive understanding of temperature-dependent optical properties is needed, especially for high-temperature applications such as thermal-photonic devices[18], thermalphotovoltaics[19] and radiative energy converters[20],

Raman and IR spectra are fundamentally connected with phonon anharmonicity of zone-center optical phonon modes. The anharmonicity is a key parameter in the complex dielectric function of polar dielectrics in the IR range, where the phonon linewidth is used in the Lorentz oscillator model[21–23]. As a result, the broadening of the spectral lines, i.e., the full width at half maximum (FWHM), is directly related to the phonon scattering rates[24]. First-principles calculation based on density functional theory (DFT) and perturbation theory is a powerful tool for understanding phonon dynamics. Without experimental fitting parameters, the zone-center optical phonon linewidth can be obtained from the phonon scattering rate. It was believed that three-phonon (3ph) scattering was adequate for predicting the phonon linewidth. However, the predicted linewidths can fall considerably below experimental data[25,26]. To include the higher-order scattering effect, several attempts have been made by using semi-empirical models for h-BN[27,28]. The higher-order anharmonic potential coefficients of perturbation theory were estimated from fits to the linewidth temperature dependence[24].

Recently, Feng and Ruan developed the general theory and computational method of four-phonon (4ph) scattering[29,30], which was subsequently confirmed by independent thermal conductivity measurements on boron arsenide[31–33]. For optical properties, it has been demonstrated that 4ph scattering plays an important role in Raman and IR spectra, especially at high-temperatures[5,34,35]. Furthermore, at finite temperatures, the interatomic force

constants (IFCs) deviate from their values at 0 K due to thermal expansion and phonon scattering, leading to the phonon renormalization effect that plays an important role in various materials[36–42]. A first-principles prediction of temperature-dependent Raman and IR linewidths requires a comprehensive understanding of all these physical phenomena.

In this work, we employ the first-principles method to predict the zone-center phonon linewidths of bulk h-BN across the temperature range of 200-600 K. Our prediction considers both 3ph and 4ph scattering mechanisms and includes phonon renormalization with the temperature-dependent effective potential (TDEP) method[36]. Our results demonstrate a significant contribution of 4ph scattering and show that considering the effect of phonon renormalization is essential for the accurate prediction of zone-center phonon linewidth as it significantly weakens phonon scattering. Neglecting the phonon renormalization mechanism would lead to a considerable overestimation of the phonon linewidth and its temperature dependency. The anisotropic dielectric functions are subsequently calculated using Lorentz model. The predicted optical properties agree with both previous experiments and our own measurements.

The complex dielectric function of h-BN in the mid-IR range is obtained from the four-parameter semi-quantum Lorentz oscillator model[21–23,43–45]:

$$\varepsilon(\omega) = \varepsilon_\infty \prod_m \left(\frac{\omega_{\mathrm{LO},m}^2 - \omega^2 - i\gamma_{\mathrm{LO},m}\omega}{\omega_{\mathrm{TO},m}^2 - \omega^2 - i\gamma_{\mathrm{TO},m}\omega} \right) \tag{1}$$

where ε_∞ is the dielectric constant at the high-frequency limit, ω is the photon frequency, $\omega_{TO,m}$ and $\gamma_{TO,m}$ are the frequency and linewidth of the m-th IR-active TO phonon, respectively. $\omega_{TO,m}$ and $\gamma_{TO,m}$ are the frequency and linewidth of the paired m-th LO phonon, respectively. m goes over all the IR-active TO phonon modes. This model is considered to be more accurate than the three-parameter model[28,43,44].

In this work, the first-principles calculations are carried out using Vienna Ab initio Simulation Package (VASP) package[46]. The lattice structure is shown in Fig. 1. A full structural relaxation leads to the lattice constants of a = 2.49 and c = 6.48 Å. The harmonic calculation at 0 K is performed using density functional perturbation theory (DFPT). Phonopy[47] is used to extract the second-order IFCs. The anharmonic IFC calculations are carried out with the finite displacement method using Thirdorder[48] and Fourthorder[49] packages.

To account for the phonon renormalization effect, we employ the TDEP method[36]. This

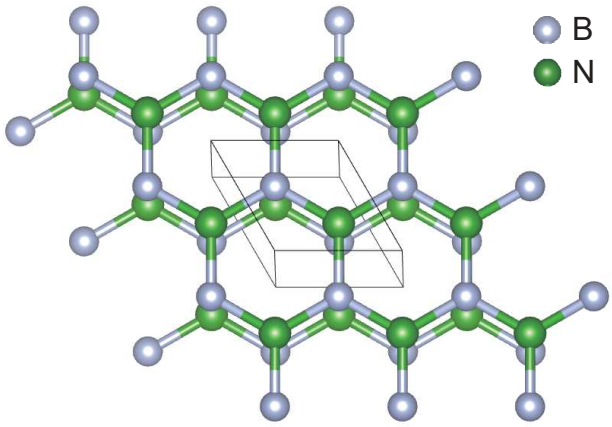

FIG. 1. **Lattice structure of bulk h-BN.** Lattice structure of h-BN, with one primitive cell shown in the black wireframe.

involves simulating a set of thermal displacements of atoms at finite temperatures based on the Bose-Einstein distribution and subsequently calculating the corresponding forces using first-principles calculations. The temperature-dependent effective IFCs are then derived by fitting the force-displacement pairs. A detailed description of this method can be found in previous works[36,50,51].

The phonon linewidth is calculated based on single-mode relaxation time approximation (SMRTA), which has been demonstrated to be valid for predicting phonon linewidth and dielectric function[25,35,52,53]. The 3ph and 4ph scattering rates are given by:

$$(\tau_\lambda^{3\mathrm{ph}})^{-1} = \frac{1}{N}\left(\sum_{\lambda'\lambda''}^{(+)} \Gamma^{(+)}_{\lambda\lambda'\lambda''} + \sum_{\lambda'\lambda''}^{(-)} \frac{1}{2}\Gamma^{(-)}_{\lambda\lambda'\lambda''}\right), \tag{2}$$

$$(\tau_\lambda^{4\mathrm{ph}})^{-1} = \frac{1}{N}\left(\sum_{\lambda'\lambda''\lambda'''}^{(++)} \frac{1}{2}\Gamma^{(++)}_{\lambda\lambda'\lambda''\lambda'''} + \sum_{\lambda'\lambda''\lambda'''}^{(+-)} \frac{1}{2}\Gamma^{(+-)}_{\lambda\lambda'\lambda''\lambda'''} + \sum_{\lambda'\lambda''\lambda'''}^{(--)} \frac{1}{6}\Gamma^{(--)}_{\lambda\lambda'\lambda''\lambda'''}\right), \tag{3}$$

where N is the total grid number of **q**-mesh and Γ terms are scattering rates which can be obtained from Fermi's golden rule[29,30,49]. In 3ph scattering, $\Gamma^{(+)}_{\lambda\lambda'\lambda''}$ and $\Gamma^{(-)}_{\lambda\lambda'\lambda''}$ represents the combination ($\lambda + \lambda' \rightarrow \lambda''$) and splitting processes ($\lambda \rightarrow \lambda' + \lambda''$), while in 4ph scattering, $\Gamma^{(++)}_{\lambda\lambda'\lambda''\lambda'''}$, $\Gamma^{(+-)}_{\lambda\lambda'\lambda''\lambda'''}$ and $\Gamma^{(--)}_{\lambda\lambda'\lambda''\lambda'''}$ represents the combination ($\lambda + \lambda' + \lambda'' \rightarrow \lambda'''$), redistribution ($\lambda + \lambda' \rightarrow \lambda'' + \lambda'''$) and splitting ($\lambda \rightarrow \lambda' + \lambda'' + \lambda'''$) processes, respectively. The total phonon scattering rate is a summation of 3ph, 4ph and isotope scattering rates based on Matthiessen's rule[54]: $\tau_\lambda^{-1} = (\tau_\lambda^{3\mathrm{ph}})^{-1} + (\tau_\lambda^{4\mathrm{ph}})^{-1} + (\tau_\lambda^{\mathrm{iso}})^{-1}$. The phonon linewidth

expressed in cm^{-1} is then proportional to the zone-center optical phonon scattering rate as $2\pi c\gamma_\lambda = \tau_\lambda^{-1}$.

All the phonon scattering calculations are performed with the ShengBTE[48] package integrated with the FourPhonon module[49]. To reduce the computational cost, we adopted a sampling-accelerated approach[55,56] to calculate 4ph scattering rates. This method estimates the phonon scattering rates based on a subset of all phonon scattering processes and works well for situations where the SMRTA is valid. More simulation details can be found in Supplementary Materials.

The experimental measurement of the $E_{2g,\mathrm{high}}$ mode linewidth is conducted between 200 K and 600 K with intervals of 100 K. The h-BN flakes are exfoliated onto a silicon wafer and characterized via AFM, indicating bulk thickness. Raman spectroscopy is conducted on the chosen flakes using a low-power laser within a high-temperature cryostation, of which Lorentzian lineshapes are fitted to the data yielding the Raman peak positions, intensities, and linewidths (see Fig. S1). More experimental details can be found in Supplementary Materials.

Symmetry analysis reveals that the irreducible representations of h-BN are $2A_{2u} + 2B_{1g} + 2E_{2g} + 2E_{1u}$, among which $2E_{2g}$ are two Raman-active modes. For phonon mode E_{1u} and A_{2u}, the transverse optical (TO) modes ($A_{2u,\mathrm{TO}}, E_{1u,\mathrm{TO}}$) are IR-active, while the paired longitudinal optical (LO) modes ($A_{2u,\mathrm{LO}}, E_{1u,\mathrm{LO}}$) would also have influence on the IR spectra. The location of these phonon modes on the phonon dispersion is shown in Fig. S2. Given that most experiments are conducted at room temperature, we first compare our results with experimental measurements and other simulations at this temperature, as summarized in Table I. Overall, our predicted phonon frequency and linewidth closely align with our own measurement and other experimental work. The minor deviations in phonon frequency may stem from the choice of pseudopotential and simulation software, which is discussed by Cigarini et al.[57]. Regarding Raman linewidth, it is worth noting that the prediction from Giles et al.[1] significantly underestimates the experimental results. This discrepancy can be attributed to their exclusion of 4ph scattering, which we have found to be responsible for around 30% of the linewidth. Additionally, it is challenging to observe the low-frequency Raman-active mode $E_{2g,\mathrm{low}}$ in Raman spectra due to its low intensity, small frequency, and extremely narrow linewidth. Consequently, the linewidth of $E_{2g,\mathrm{low}}$ has not been reported in past Raman measurements that have been focused on the high-frequency Raman-active

TABLE I. Phonon frequencies ω (cm^{-1}) and linewidths γ (cm^{-1}) of zone-center phonon modes at 300 K, compared to the values from other experiments and theory.

Summary		Theory (This work)	Theory (Literature)	Experiments
Raman-active modes	$\omega_{E_{2g,high}}$	1376	1354-1384[57,59]	1364-1376[13,16,27,60], 1368 (This work)
	$\omega_{E_{2g,low}}$	42	37-50[57]	51[27], 52[60]
	$\gamma_{E_{2g,high}}$,	7.54	4.14[1]	7.7[27], 8.5[1], 7.7±0.1 (This work)
	$\gamma_{E_{2g,low}}$	0.31	–	–
IR-active TO modes and paired LO modes	$\omega_{E_{1u,LO}}$	1614	1573-1629[15,57,59]	1605-1623[4,13,15,16,28,59]
	$\omega_{E_{1u,TO}}$	1364	1354-1384[15,57,59]	1365-1370[4,13,15,16,28,59,61–66]
	$\omega_{A_{2u,LO}}$	825	810[59], 818[15]	820-828[4,13,15,59]
	$\omega_{A_{2u,TO}}$	760	741-756[15,57,59]	760-810[4,13,15,59,61–66]
	$\gamma_{E_{1u,LO}}$	4.07	–	3.8[28]
	$\gamma_{E_{1u,TO}}$	5.49	–	6.4-7.1[1,28,58]
	$\gamma_{A_{2u,LO}}$	1.34	–	–
	$\gamma_{A_{2u,TO}}$	2.03	–	2[58], 2.2[1]

mode $E_{2g,high}$. Turning to the IR-active TO modes and the paired LO modes, Ref.[28] obtained both γ_{LO} and γ_{TO} by fitting the experimental result to Eq. 1, while Ref.[1,58] only obtained γ_{TO} since they fit the experimental results to the three-parameter classical Lorentz model, given by: $\varepsilon(\omega) = \varepsilon_\infty \left(1 + \sum_m \frac{\omega_{LO,m}^2 - \omega_{TO,m}^2}{\omega_{TO,m}^2 - \omega^2 - i\gamma_{TO,m}\omega}\right)$. Our predicted linewidths are in good agreement with the experiments. Besides, most theoretical studies focus on the zone-center optical phonon frequency, while the phonon linewidth is not addressed adequately in theoretical works. Our study addresses this knowledge gap by focusing on phonon linewidth calculations.

We now discuss the temperature dependency of Raman linewidth and the impact of 4ph scattering and phonon renormalization. As shown in Fig. 2a, the predicted $\gamma_{E_{2g,high}}$ using only 3ph scattering without phonon renormalization shows a linear relationship with temperature and notably underestimates the experimental results. After incorporating 4ph scattering, the predicted linewidth increases considerably, indicating a strong 4ph scattering effect. However, the predicted total linewidth is much higher than the experimental results and shows a much stronger temperature dependence. After we further include the phonon

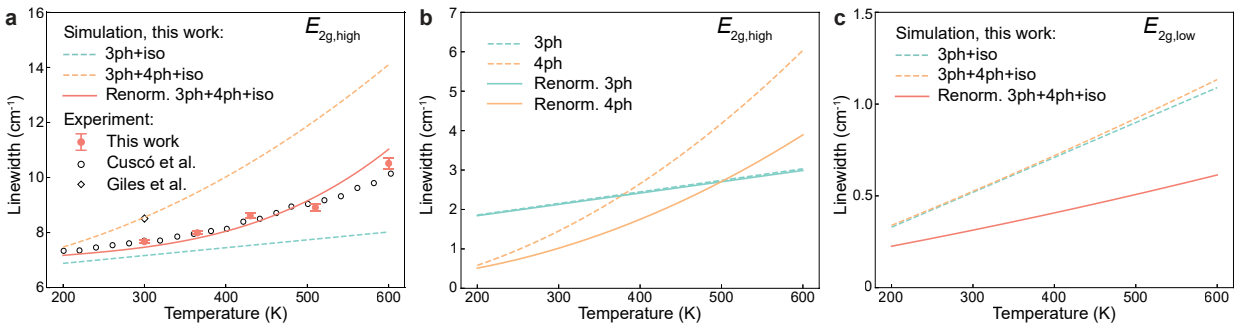

FIG. 2. **Temperature-dependent phonon linewidth of Raman-active modes. a,** $\gamma_{E_{2g,high}}$. **b,** Comparison of contribution of 3ph and 4ph scattering to $\gamma_{E_{2g,high}}$. **c,** $\gamma_{E_{2g,low}}$. Experimental values are from Ref.[1,27] and our measurement.

renormalization effect, we observe a reduction in the linewidth of $E_{2g,high}$ and a weakening of the temperature dependency, agreeing much better with our experimental results which contain appreciable uncertainties because of the relatively weak Raman signal from h-BN far from resonant conditions[16], as compared to typical signals from graphene and TMDs observed near resonance. We also see that the contribution of 4ph scattering exceeds 3ph scattering at high temperatures (Fig. 2b). This observation reveals the important roles played by both 4ph scattering and phonon renormalization in influencing the Raman phonon linewidth, particularly at elevated temperatures. On the other hand, the $E_{2g,low}$ phonon mode shows a minor influence from 4ph scattering, and the predicted linewidth is further reduced after incorporating the phonon renormalization effect, as shown in Fig. 2c. Note that the linewidth of $E_{2g,low}$ phonon mode is much lower than that of the $E_{2g,high}$ mode and is less affected by 4ph scattering. This can be attributed to its lower phonon frequency compared to the $E_{2g,high}$ mode, which reduces the available decay channels and limits its scattering rate. Generally, the scattering rate follows $(\tau_\lambda^{3ph})^{-1} \sim \omega^2$ for 3ph scattering and $(\tau_\lambda^{3ph})^{-1} \sim \omega^4$ for 4ph scattering. We also compared the frequency shift of $E_{2g,low}$ against the experimental results from the literature[67], as illustrated in Fig. S3.

Figure 3 shows the temperature-dependent linewidths for the IR-active TO modes and the paired LO modes. Similar to our observations of Raman-active modes, the inclusion of the 4ph scattering effect significantly increases the linewidths for these modes and enhances their temperature dependency. Subsequently, when we account for the phonon renormalization effect, the linewidths are reduced. Specifically, the predicted $\gamma_{E_{1u,LO}}$ agrees well with

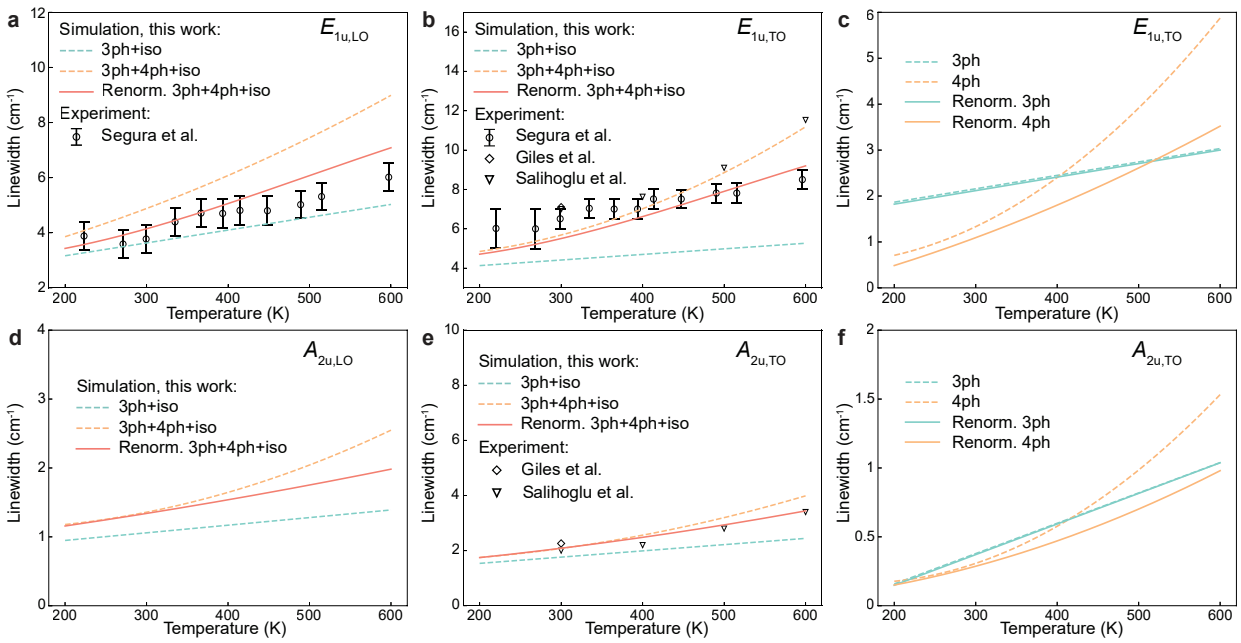

FIG. 3. **Temperature-dependent phonon linewidth of the IR-active TO modes and the paired LO modes.** **a,** $\gamma_{E_{1u,LO}}$. **b,** $\gamma_{E_{1u,TO}}$. **c,** Comparison of contribution of 3ph and 4ph scattering to $\gamma_{E_{1u,TO}}$. **d,** $\gamma_{A_{2u,LO}}$. **e,** $\gamma_{A_{2u,TO}}$. **f,** Comparison of contribution of 3ph and 4ph scattering to $\gamma_{A_{2u,TO}}$. Experimental values are from Ref.[1,28,58].

the experimental results (Fig. 3a). As for $\gamma_{E_{1u,TO}}$, our prediction is in good agreement with the experimental results from Segura et al.[28], while slightly lower than the experimental data from Salihoglu et al.[58], likely due to defects and impurities in experiments that result in additional phonon scattering (Fig. 3b). However, the temperature dependence of our prediction and the experimental results are close, while the result without phonon renormalization shows a stronger temperature dependency. In the case of the $A_{2u,LO}$ and $A_{2u,TO}$ modes, Figs. 3d and e illustrate our predicted linewidths. The prediction of $\gamma_{A_{2u,TO}}$ has a consistent trend with the experimental result. We also note that 4ph scattering shows significant or even leading contributions to the linewidths, especially at high temperatures, as shown in Figs. 3c and f.

After obtaining the linewidths of IR-active phonon modes, we can now predict the anisotropic dielectric function of h-BN using Lorentz model. Since there are already extensive studies on the zone-center optical phonon frequency of h-BN and the simulation value is known to vary with different pseudopotentials[57], we take the experimental value

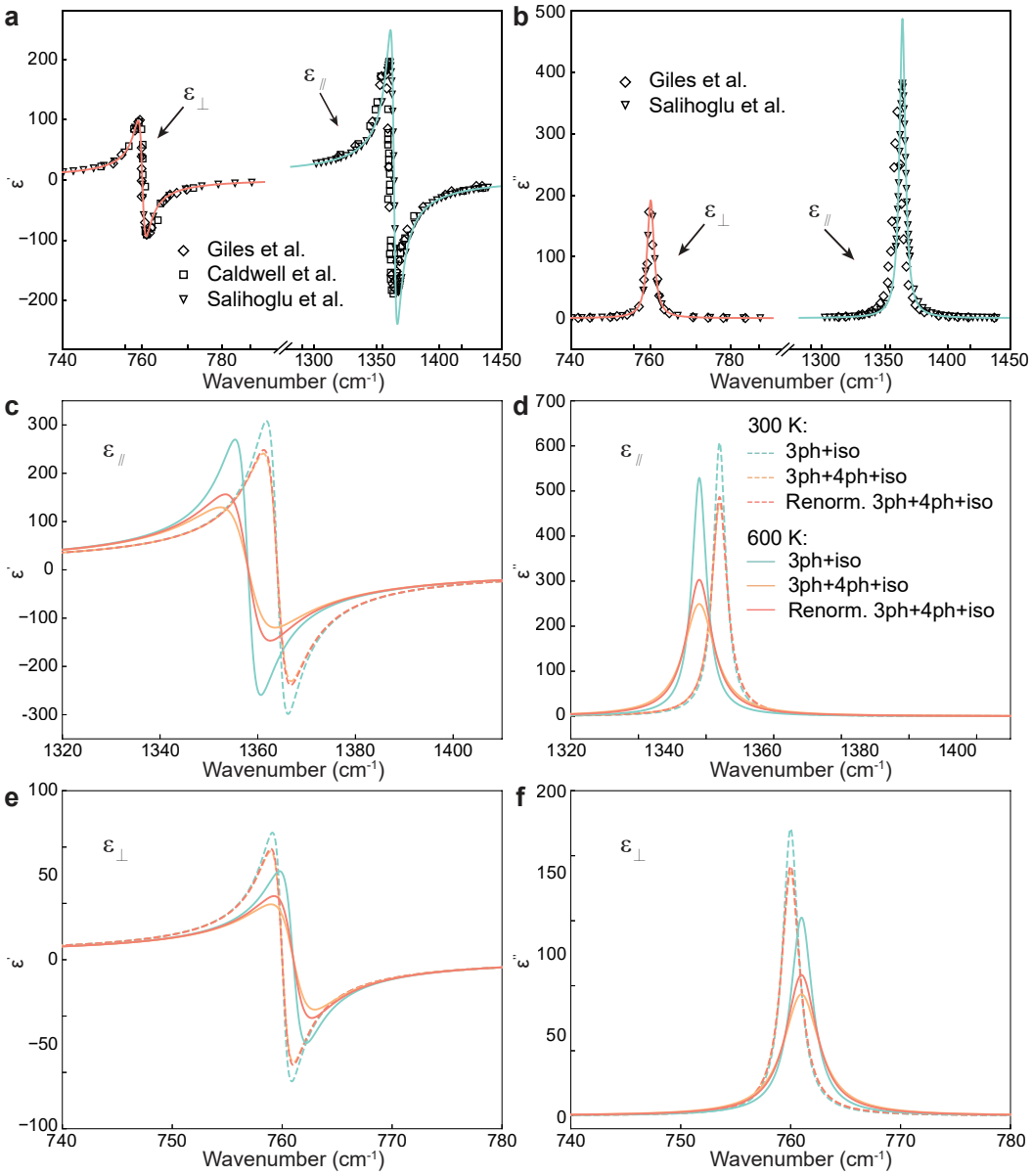

FIG. 4. **Anisotropic dielectric function. a, b,** The prediction of $\varepsilon_{\parallel}$ and $\varepsilon_{\perp}$ at 300 K compared with experiments[1,4,58]. Figures **a** and **b** are for the real and imaginary parts of the dielectric functions, respectively. **c-f,** The prediction of dielectric functions at 300 K (dash line) and 600 K (solid line) considering only 3ph scattering, 3ph+4ph scattering and 3ph+4ph scattering with phonon renormalization effect. Figures **c** and **d** are for $\varepsilon_{\parallel}$ and figures **e** and **f** are for $\varepsilon_{\perp}$.

of the phonon frequencies from prior experiment[58] combined with our predicted linewidths. Figures 4a and b show the dielectric functions in parallel (E ∥ c-axis) and perpendicular (E ⊥ c-axis) direction at 300 K along with a comparison to experimental results. Our predictions

align well with the experimental results. Furthermore, while the impact of 4ph scattering and phonon renormalization is relatively weak at room temperature, it becomes significant at higher temperatures, as depicted in Figs. 4c-f. We also calculate the temperature-dependent dielectric function, which is shown in Fig. S4.

In summary, this study employs first-principles calculations to predict the temperature-dependent linewidths of zone-center phonon modes and the dielectric function in bulk h-BN. Notably, we incorporate the contributions of four-phonon scattering and phonon renormalization that have not been accounted for in prior reports. The predicted phonon linewidth and dielectric function agree with the experimental results. Furthermore, our investigation reveals the competing effects of four-phonon scattering and phonon renormalization in the Raman and IR linewidths of h-BN, particularly at elevated temperatures.

SUPPLEMENTARY MATERIAL

See Supplementary Material for simulation and experimental details, Raman spectra, phonon dispersion, frequency shift of Raman mode, and temperature-dependent dielectric function.

DATA AVAILABILITY

The original results of the study are available from the corresponding authors upon reasonable request.

ACKNOWLEDGMENTS

X.R., Z.H., and L.S., P.S. were supported by two collaborating Grants (No. 2321301 and No. 2321302) of the U.S. National Science Foundation. Z.G. was supported by Award No. 2102645 of the U.S. National Science Foundation. Z.G. acknowledges the Ross Fellowship from Purdue University. K.W. and T.T. acknowledge support from the JSPS KAKENHI (Grant Numbers 21H05233 and 23H02052) and World Premier International Research Center Initiative (WPI), MEXT, Japan. Simulations were performed at the Rosen Center for Advanced Computing (RCAC) of Purdue University. Growth of hBN crystals was supported by JSPS KAKENHI (Grant Numbers 19H05790, 20H00354 and 21H05233).

COMPETING INTERESTS

The authors declare no competing interests.

AUTHOR CONTRIBUTIONS

X.R. and Z.G. conceived the study. Z.G. designed and did the simulations, analyzed the results, and wrote the manuscript. Z.H. and Y.C helped with the simulation and data analysis. P.S. was advised by L.S. to measure the Raman linewidth. T.T. and K.W. synthesized the hBN crystals. X.R. supervised the project. All authors contributed to discussions and revisions of the manuscript.

REFERENCES

[1]A. J. Giles, S. Dai, I. Vurgaftman, T. Hoffman, S. Liu, L. Lindsay, C. T. Ellis, N. Assefa, I. Chatzakis, T. L. Reinecke, *et al.*, "Ultralow-loss polaritons in isotopically pure boron nitride," Nature Materials **17**, 134–139 (2018).

[2]E. Yoxall, M. Schnell, A. Y. Nikitin, O. Txoperena, A. Woessner, M. B. Lundeberg, F. Casanova, L. E. Hueso, F. H. Koppens, and R. Hillenbrand, "Direct observation of ultraslow hyperbolic polariton propagation with negative phase velocity," Nature Photonics **9**, 674–678 (2015).

[3]P. Li, M. Lewin, A. V. Kretinin, J. D. Caldwell, K. S. Novoselov, T. Taniguchi, K. Watanabe, F. Gaussmann, and T. Taubner, "Hyperbolic phonon-polaritons in boron nitride for near-field optical imaging and focusing," Nature Communications **6**, 7507 (2015).

[4]J. D. Caldwell, A. V. Kretinin, Y. Chen, V. Giannini, M. M. Fogler, Y. Francescato, C. T. Ellis, J. G. Tischler, C. R. Woods, A. J. Giles, *et al.*, "Sub-diffractional volume-confined polaritons in the natural hyperbolic material hexagonal boron nitride," Nature Communications **5**, 5221 (2014).

[5]D. Xiang, T. Liu, J. Xu, J. Y. Tan, Z. Hu, B. Lei, Y. Zheng, J. Wu, A. C. Neto, L. Liu, *et al.*, "Two-dimensional multibit optoelectronic memory with broadband spectrum distinction," Nature Communications **9**, 2966 (2018).

[6]N. Mendelson, M. Doherty, M. Toth, I. Aharonovich, and T. T. Tran, "Strain-induced modification of the optical characteristics of quantum emitters in hexagonal boron nitride," Advanced Materials **32**, 1908316 (2020).

[7]J. D. Caldwell, I. Aharonovich, G. Cassabois, J. H. Edgar, B. Gil, and D. Basov, "Photonics with hexagonal boron nitride," Nature Reviews Materials **4**, 552–567 (2019).

[8]Y. Kubota, K. Watanabe, O. Tsuda, and T. Taniguchi, "Deep ultraviolet light-emitting hexagonal boron nitride synthesized at atmospheric pressure," Science **317**, 932–934 (2007).

[9]G. Grosso, H. Moon, B. Lienhard, S. Ali, D. K. Efetov, M. M. Furchi, P. Jarillo-Herrero, M. J. Ford, I. Aharonovich, and D. Englund, "Tunable and high-purity room temperature single-photon emission from atomic defects in hexagonal boron nitride," Nature Communications **8**, 1–8 (2017).

[10]M. Kianinia, C. Bradac, B. Sontheimer, F. Wang, T. T. Tran, M. Nguyen, S. Kim, Z.-Q. Xu, D. Jin, A. W. Schell, *et al.*, "All-optical control and super-resolution imaging of quantum emitters in layered materials," Nature Communications **9**, 874 (2018).

[11]D. R. Danielsen, A. Lyksborg-Andersen, K. E. Nielsen, B. S. Jessen, T. J. Booth, M.-H. Doan, Y. Zhou, P. Bøggild, and L. Gammelgaard, "Super-resolution nanolithography of two-dimensional materials by anisotropic etching," ACS Applied Materials & Interfaces **13**, 41886–41894 (2021).

[12]A. Felicelli, I. Katsamba, F. Barrios, Y. Zhang, Z. Guo, J. Peoples, G. Chiu, and X. Ruan, "Thin layer lightweight and ultrawhite hexagonal boron nitride nanoporous paints for daytime radiative cooling," Cell Reports Physical Science **3** (2022).

[13]R. Geick, C. Perry, and G. Rupprecht, "Normal modes in hexagonal boron nitride," Physical Review **146**, 543 (1966).

[14]H. Akbari, W.-H. Lin, B. Vest, P. K. Jha, and H. A. Atwater, "Temperature-dependent spectral emission of hexagonal boron nitride quantum emitters on conductive and dielectric substrates," Physical Review Applied **15**, 014036 (2021).

[15]A. Segura, R. Cuscó, T. Taniguchi, K. Watanabe, G. Cassabois, B. Gil, and L. Artús, "High-pressure softening of the out-of-plane a2u (transverse-optic) mode of hexagonal boron nitride induced by dynamical buckling," The Journal of Physical Chemistry C **123**, 17491–17497 (2019).

[16]S. Reich, A. Ferrari, R. Arenal, A. Loiseau, I. Bello, and J. Robertson, "Resonant raman scattering in cubic and hexagonal boron nitride," Physical Review B **71**, 205201 (2005).

[17]H. Fujiwara, *Spectroscopic ellipsometry: principles and applications* (John Wiley & Sons, 2007).

[18]D. Feng, S. K. Yee, and Z. M. Zhang, "Near-field photonic thermal diode based on hbn and insb films," Applied Physics Letters **119**, 181111 (2021).

[19]R. Messina and P. Ben-Abdallah, "Graphene-based photovoltaic cells for near-field thermal energy conversion," Scientific Reports **3**, 1383 (2013).

[20]D. Feng, X. Ruan, S. K. Yee, and Z. M. Zhang, "Thermoradiative devices enabled by hyperbolic phonon polaritons at nanoscales," Nano Energy **103**, 107831 (2022).

[21]M. Born, K. Huang, and M. Lax, "Dynamical theory of crystal lattices," American Journal of Physics **23**, 474–474 (1955).

[22]A. Barker Jr, "Transverse and longitudinal optic mode study in mgf2 and znf2," Physical Review **136**, A1290 (1964).

[23]F. Gervais and B. Piriou, "Anharmonicity in several-polar-mode crystals: adjusting phonon self-energy of lo and to modes in al2o3 and tio2 to fit infrared reflectivity," Journal of Physics C: Solid State Physics **7**, 2374 (1974).

[24]R. A. Cowley, "Anharmonic crystals," Reports on Progress in Physics **31**, 123 (1968).

[25]A. Debernardi, S. Baroni, and E. Molinari, "Anharmonic phonon lifetimes in semiconductors from density-functional perturbation theory," Physical Review Letters **75**, 1819 (1995).

[26]A. Debernardi, "Phonon linewidth in iii-v semiconductors from density-functional perturbation theory," Physical Review B **57**, 12847 (1998).

[27]R. Cuscó, B. Gil, G. Cassabois, and L. Artús, "Temperature dependence of raman-active phonons and anharmonic interactions in layered hexagonal bn," Physical Review B **94**, 155435 (2016).

[28]A. Segura, R. Cuscó, T. Taniguchi, K. Watanabe, and L. Artús, "Long lifetime of the e 1 u in-plane infrared-active modes of h-bn," Physical Review B **101**, 235203 (2020).

[29]T. Feng, L. Lindsay, and X. Ruan, "Four-phonon scattering significantly reduces intrinsic thermal conductivity of solids," Physical Review B **96**, 161201 (2017).

[30]T. Feng and X. Ruan, "Quantum mechanical prediction of four-phonon scattering rates and reduced thermal conductivity of solids," Physical Review B **93**, 045202 (2016).

[31]J. S. Kang, M. Li, H. Wu, H. Nguyen, and Y. Hu, "Experimental observation of high thermal conductivity in boron arsenide," Science **361**, 575–578 (2018).

[32]F. Tian, B. Song, X. Chen, N. K. Ravichandran, Y. Lv, K. Chen, S. Sullivan, J. Kim, Y. Zhou, T.-H. Liu, *et al.*, "Unusual high thermal conductivity in boron arsenide bulk crystals," Science **361**, 582–585 (2018).

[33]S. Li, Q. Zheng, Y. Lv, X. Liu, X. Wang, P. Y. Huang, D. G. Cahill, and B. Lv, "High thermal conductivity in cubic boron arsenide crystals," Science **361**, 579–581 (2018).

[34]Z. Tong, X. Yang, T. Feng, H. Bao, and X. Ruan, "First-principles predictions of temperature-dependent infrared dielectric function of polar materials by including four-phonon scattering and phonon frequency shift," Physical Review B **101**, 125416 (2020).

[35]X. Yang, T. Feng, J. S. Kang, Y. Hu, J. Li, and X. Ruan, "Observation of strong higher-order lattice anharmonicity in raman and infrared spectra," Physical Review B **101**, 161202 (2020).

[36]O. Hellman, I. Abrikosov, and S. Simak, "Lattice dynamics of anharmonic solids from first principles," Physical Review B **84**, 180301 (2011).

[37]F. Zhou, W. Nielson, Y. Xia, V. Ozoliņš, *et al.*, "Lattice anharmonicity and thermal conductivity from compressive sensing of first-principles calculations," Physical Review Letters **113**, 185501 (2014).

[38]Y. Xia, "Revisiting lattice thermal transport in pbte: The crucial role of quartic anharmonicity," Applied Physics Letters **113** (2018).

[39]N. K. Ravichandran and D. Broido, "Unified first-principles theory of thermal properties of insulators," Physical Review B **98**, 085205 (2018).

[40]A. Jain, "Multichannel thermal transport in crystalline tl 3 vse 4," Physical Review B **102**, 201201 (2020).

[41]Y. Xia, K. Pal, J. He, V. Ozoliņš, and C. Wolverton, "Particlelike phonon propagation dominates ultralow lattice thermal conductivity in crystalline tl 3 vse 4," Physical Review Letters **124**, 065901 (2020).

[42]Z. Guo, Z. Han, A. Alkandari, K. Khot, and X. Ruan, "First-principles prediction of thermal conductivity of bulk hexagonal boron nitride," Applied Physics Letters **124** (2024).

[43]R. Lowndes, "Influence of lattice anharmonicity on the longitudinal optic modes of cubic ionic solids," Physical Review B **1**, 2754 (1970).

[44]M. Schubert, T. Tiwald, and C. Herzinger, "Infrared dielectric anisotropy and phonon modes of sapphire," Physical Review B **61**, 8187 (2000).

[45]D. W. Berreman and F. Unterwald, "Adjusting poles and zeros of dielectric dispersion to fit reststrahlen of pr cl 3 and la cl 3," Physical Review **174**, 791 (1968).

[46]G. Kresse and J. Furthmüller, "Efficient iterative schemes for ab initio total-energy calculations using a plane-wave basis set," Physical Review B **54**, 11169 (1996).

[47]A. Togo and I. Tanaka, "First principles phonon calculations in materials science," Scripta Materialia **108**, 1–5 (2015).

[48]W. Li, J. Carrete, N. A. Katcho, and N. Mingo, "Shengbte: A solver of the boltzmann transport equation for phonons," Computer Physics Communications **185**, 1747–1758 (2014).

[49]Z. Han, X. Yang, W. Li, T. Feng, and X. Ruan, "Fourphonon: An extension module to shengbte for computing four-phonon scattering rates and thermal conductivity," Computer Physics Communications **270**, 108179 (2022).

[50]O. Hellman, P. Steneteg, I. A. Abrikosov, and S. I. Simak, "Temperature dependent effective potential method for accurate free energy calculations of solids," Physical Review B **87**, 104111 (2013).

[51]O. Hellman and I. A. Abrikosov, "Temperature-dependent effective third-order interatomic force constants from first principles," Physical Review B **88**, 144301 (2013).

[52]A. Maradudin and A. Fein, "Scattering of neutrons by an anharmonic crystal," Physical Review **128**, 2589 (1962).

[53]Z. Tong, J. Peoples, X. Li, X. Yang, H. Bao, and X. Ruan, "Electronic and phononic origins of baso4 as an ultra-efficient radiative cooling paint pigment," Materials Today Physics **24**, 100658 (2022).

[54]J. Ziman, *Electrons and Phonons: The Theory of Transport Phenomena in Solids* (Oxford University Press, Northamptonshire, 2001).

[55]Z. Guo, Z. Han, D. Feng, G. Lin, and X. Ruan, "Sampling-accelerated prediction of phonon scattering rates for converged thermal conductivity and radiative properties," npj Computational Materials **10**, 31 (2024).

[56]Z. Guo, P. Roy Chowdhury, Z. Han, Y. Sun, D. Feng, G. Lin, and X. Ruan, "Fast and accurate machine learning prediction of phonon scattering rates and lattice thermal conductivity," npj Computational Materials **9**, 95 (2023).

[57]L. Cigarini, M. Novotnỳ, and F. Karlickỳ, "Lattice dynamics in the conformational environment of multilayered hexagonal boron nitride (h-bn) results in peculiar infrared optical responses," Physical Chemistry Chemical Physics **23**, 7247–7260 (2021).

[58]H. Salihoglu, V. Iyer, T. Taniguchi, K. Watanabe, P. D. Ye, and X. Xu, "Energy transport by radiation in hyperbolic material comparable to conduction," Advanced Functional Materials **30**, 1905830 (2020).

[59]J. Serrano, A. Bosak, R. Arenal, M. Krisch, K. Watanabe, T. Taniguchi, H. Kanda, A. Rubio, and L. Wirtz, "Vibrational properties of hexagonal boron nitride: inelastic x-ray scattering and ab initio calculations," Physical Review Letters **98**, 095503 (2007).

[60]R. Nemanich, S. Solin, and R. M. Martin, "Light scattering study of boron nitride microcrystals," Physical Review B **23**, 6348 (1981).

[61]A. Hidalgo, V. Makarov, G. Morell, B. Weiner, *et al.*, "High-yield synthesis of cubic and hexagonal boron nitride nanoparticles by laser chemical vapor decomposition of borazine," Dataset Papers in Science **2013** (2012).

[62]H. E. Çamurlu, S. Mathur, O. Arslan, and E. Akarsu, "Modification of hexagonal boron nitride nanoparticles with fluorosilane," Ceramics International **42**, 6312–6318 (2016).

[63]A. Mukheem, S. Shahabuddin, N. Akbar, A. Miskon, N. Muhamad Sarih, K. Sudesh, N. Ahmed Khan, R. Saidur, and N. Sridewi, "Boron nitride doped polyhydroxyalkanoate/chitosan nanocomposite for antibacterial and biological applications," Nanomaterials **9**, 645 (2019).

[64]L. Chen, H.-F. Xu, S.-J. He, Y.-H. Du, N.-J. Yu, X.-Z. Du, J. Lin, and S. Nazarenko, "Thermal conductivity performance of polypropylene composites filled with polydopamine-functionalized hexagonal boron nitride," PloS one **12**, e0170523 (2017).

[65]X. Wang, Y. Xie, and Q. Guo, "Synthesis of high quality inorganic fullerene-like bn hollow spheres via a simple chemical route," Chemical Communications , 2688–2689 (2003).

[66]J. Andujar, E. Bertran, and M. Polo, "Plasma-enhanced chemical vapor deposition of boron nitride thin films from b2h6–h2–nh3 and b2h 6–n2 gas mixtures," Journal of Vacuum Science & Technology A: Vacuum, Surfaces, and Films **16**, 578–586 (1998).

[67]R. Cuscó, J. H. Edgar, S. Liu, G. Cassabois, B. Gil, and L. Artús, "Influence of isotopic substitution on the anharmonicity of the interlayer shear mode of h-bn," Physical Review B **99**, 085428 (2019).